1-1-2019

Platinum/Nickel Bicarbonate Heterostructures towards Accelerated Hydrogen Evolution under Alkaline Conditions

Mengmeng Lao
University of Wollongong, ml590@uowmail.edu.au

Kun Rui
University of Wollongong, krui@uow.edu.au

Guoqiang Zhao
University of Wollongong, gz815@uowmail.edu.au

Peixin Cui
Chinese Academy Of Sciences

Xusheng Zheng
University of Science and Technology of China

See next page for additional authors

Platinum/Nickel Bicarbonate Heterostructures towards Accelerated Hydrogen Evolution under Alkaline Conditions

Abstract

Heterostructured nanomaterials, generally have physicochemical properties that differ from those of the individual components, and thus have potential in a wide range of applications. New platinum (Pt)/nickel bicarbonate (Ni(HCO 3) 2) heterostructures are designed for an efficient alkaline hydrogen evolution reaction (HER). Notably, the specific and mass activity of Pt in Pt/Ni(HCO 3) 2 are substantially improved compared to the bare Pt nanoparticles (NPs). The Ni(HCO 3) 2 provides abundant water adsorption/ dissociation sites and modulate the electronic structure of Pt, which determine the elementary reaction kinetics of alkaline HER. The Ni(HCO 3) 2 nanoplates offer a platform for the uniform dispersion of Pt NPs, ensuring the maximum exposure of active sites. The results demonstrate that, Ni(HCO 3) 2 is an effective catalyst promoter for alkaline HER.

Disciplines

Engineering | Physical Sciences and Mathematics

Publication Details

Lao, M., Rui, K., Zhao, G., Cui, P., Zheng, X., Dou, S. Xue. & Sun, W. (2019). Platinum/Nickel Bicarbonate Heterostructures towards Accelerated Hydrogen Evolution under Alkaline Conditions. Angewandte Chemie - International Edition, 58 (16), 5432-5437.

Authors

Mengmeng Lao, Kun Rui, Guoqiang Zhao, Peixin Cui, Xusheng Zheng, Shi Xue Dou, and Wenping Sun

COMMUNICATION

Platinum/Nickel Bicarbonate Heterostructures towards Accelerated Hydrogen Evolution under Alkaline Conditions

Mengmeng Lao, Kun Rui, Guoqiang Zhao, Peixin Cui, Xusheng Zheng,* Shi Xue Dou and Wenping Sun*

Abstract: Heterostructured nanomaterials, generally have physicochemical properties that differ from those of the individual components, and thus have potential in a wide range of applications. New platinum (Pt)/nickel bicarbonate ($Ni(HCO_3)_2$) heterostructures are designed for an efficient alkaline hydrogen evolution reaction (HER). Notably, the specific and mass activity of Pt in $Pt/Ni(HCO_3)_2$ are substantially improved compared to the bare Pt nanoparticles (NPs). The $Ni(HCO_3)_2$ provides abundant water adsorption/dissociation sites and modulate the electronic structure of Pt, which determine the elementary reaction kinetics of alkaline HER. The $Ni(HCO_3)_2$ nanoplates offer a platform for the uniform dispersion of Pt NPs, ensuring the maximum exposure of activesites. The results demonstrate that, $Ni(HCO_3)_2$ is an effectivecatalyst promoter for alkaline HER.

Heterostructures, which are composed of at least two components, usually possess unique multifunctional physicochemical properties different from the individual components.[1] In particular, two-dimensional (2D) materials-based heterostructures with high surface-to-volume ratio, are able to achieve maximum exposure of surface atoms (active sites) and substantially shorten the pathway for charge transfer and mass diffusion.[1-2] In addition, the electron redistribution at the interface of the heterostructures is very beneficial to enhance the reaction kinetics.[1] Thus, they show great application potential in energy storage and conversion fields, such as batteries[3] and photoelectro-catalysis.[4]

Water electrolysis is a promising technology towards efficient utilization of intermittent renewable energies, and developing efficient electrocatalysts for HER and oxygen evolution reaction (OER) is vital to the substantial application of water electrolysis. Among various HER catalysts, Pt is currently proved as the most efficient one in acidic medium.[5] However, the HER kinetics in alkaline medium is severely reduced due to the sluggish water dissociation step.[6] Therefore, improving water adsorption/dissociation ability be the top priority towards enhanced alkaline HER kinetics. It was found that some transition metal oxides/hydroxides are capable of cleaving H–OH bond.[7] Markovic et al. pioneered $Ni(OH)_2$ as an efficient promoter for Pt and several other metal catalysts to improve their alkaline HER activity.[8] Theoretical calculations have also indicated that the interface of the heterostructures consumes lower energy to cleave the H–OH bond than their single counterparts.[9]

Recently, we found that $Ni(HCO_3)_2$ shows comparable OER activity to $Ni(OH)_2$ in alkaline medium (Figure S1, Supporting Information), which process is closely associated with OH^- adsorption.[10] Besides, a number of hydrophilic groups in $Ni(HCO_3)_2$, such as C–O and C=O, can interact with H_2O via hydrogen bonding, thereby favouring H_2O adsorption.[11] On this basis, we speculate that $Ni(HCO_3)_2$ might work as an efficient catalyst promoter for alkaline HER. To verify this hypothesis, $Pt/Ni(HCO_3)_2$ heterostructures with Pt NPs anchored on $Ni(HCO_3)_2$ nanoplates are synthesized, which demonstrate considerably enhanced alkaline HER catalytic activity and stability over bare Pt NPs and commercial 10 wt% Pt/C. The novel $Pt/Ni(HCO_3)_2$ heterostructure also expands the heterostructure family based on 2D materials for a variety of energy applications.

$Pt/Ni(HCO_3)_2$ heterostructures are synthesized via a facile two-step process, as illustrated in **Figure 1**a. Typically, $Ni(HCO_3)_2$ nanoplates (Figure S2) are synthesized by a hydrothermal reaction method, then Pt NPs are deposited on $Ni(HCO_3)_2$ via a solution-phase process (the detailed information is provided in Supporting Information). Figure 1b is a transmission electron microscope (TEM) image of 20% $Pt/Ni(HCO_3)_2$. It is clear that Pt NPs (2-3 nm, Figure 1c) are uniformly anchored on $Ni(HCO_3)_2$. The high-resolution TEM (HRTEM) image (Figure 1d) shows an overlapping of lattice fringes of Pt and $Ni(HCO_3)_2$. The lattice spacings of 2.4 Å can be ascribed to the (222) planes of $Ni(HCO_3)_2$. The lattice spacings of 2.2 and 1.96 Å correspond to Pt (111) and (200) planes, respectively. The fast Fourier transformation (FFT) pattern (Figure 1e) presents clear reflections of Pt (111) and (200) planes and $Ni(HCO_3)_2$ (222) planes, confirming the presence of Pt and $Ni(HCO_3)_2$. Besides, it appears that the deposition of Pt NPs does not change the morphology and crystal structure of $Ni(HCO_3)_2$ (Figure S2 and S3). In contrast, bare Pt NPs (3-6 nm) agglomerated severely in the absence of $Ni(HCO_3)_2$ (Figure S4). The results indicate that the interaction between Pt and $Ni(HCO_3)_2$ can greatly prevent the growth and aggregation of Pt NPs. In addition, the TEM images of 9% $Pt/Ni(HCO_3)_2$ and 5% $Pt/Ni(HCO_3)_2$ (Figure S5 and S6) together

[*] M. Lao, Dr. K. Rui, G. Zhao, Prof. S. X. Dou, Dr. W. Sun
Institute for Superconducting and Electronic Materials
Australian Institute for Innovative Materials
University of Wollongong,
Wollongong, NSW 2522, Australia
E-mail: wenping@uow.edu.au
Dr. X. Zheng
National Synchrotron Radiation Laboratory
University of Science and Technology of China
Hefei, 230029, P. R. China
E-mail: zxs@ustc.edu.cn
Dr. P. Cui
Key Laboratory of Soil Environment and Pollution Remediation
Institute of Soil Science, Chinese Academy of Sciences
Nanjing 210008, P. R. China

Supporting information for this article is given via a link at the end of the document.

with those of 20% Pt/Ni$(HCO_3)_2$ suggest that the size of Pt NPs increases accordingly with increasing Pt loading.

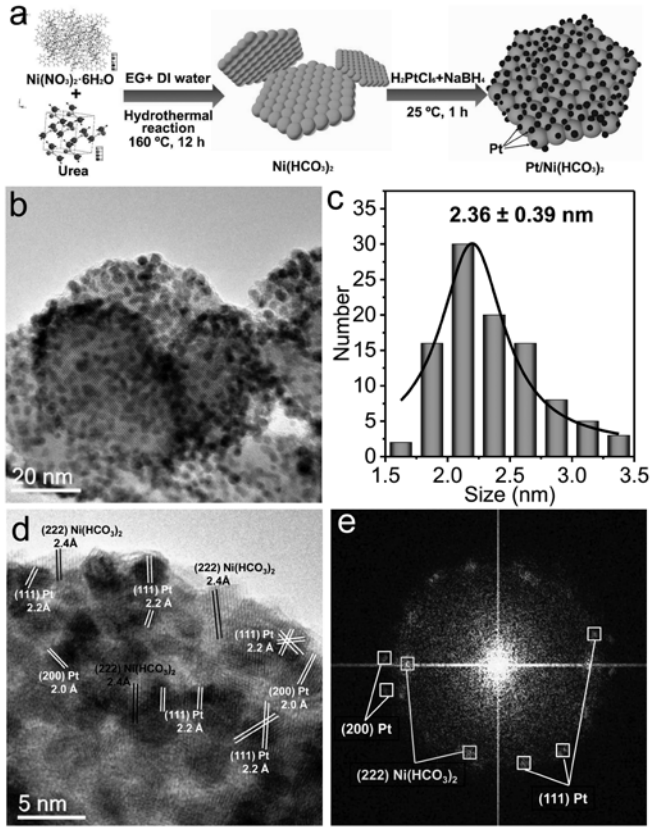

Figure 1. a) Schematic illustration of the synthesis process of Pt/Ni$(HCO_3)_2$ heterostructures. b) TEM image, c) the corresponding Pt NPs size distribution histogram, d) HRTEM image of 20% Pt/Ni$(HCO_3)_2$ heterostructure and e) the FFT-generated image derived from (d).

Figure 2a shows the X-ray diffraction (XRD) patterns of the samples. The diffraction peaks of Ni$(HCO_3)_2$ and Pt can be indexed to cubic-phased Ni$(HCO_3)_2$ (JCPDS 15-0782) and cubic-phased Pt (JCPDS 04-0802), respectively. For the Pt/Ni$(HCO_3)_2$ heterostructures, all the diffraction peaks can also be well indexed. The peak overlapping of Ni$(HCO_3)_2$ (321) planes and Pt (111) planes induces the broadened diffraction peak at around 40º. And the relative peak intensity decrease of the heterostructures might be induced by the slight surface reduction during the Pt deposition process. The chemical composition of the Pt/Ni$(HCO_3)_2$ heterostructures were further probed by X-ray photoelectron spectroscopy (XPS). The XPS survey spectra of Ni$(HCO_3)_2$ and Pt/Ni$(HCO_3)_2$ heterostructures (Figure S7a-c) confirm the existence of Ni, C, O and/or Pt elements. Deconvolution of the high-resolution XPS spectrum of Pt 4f doublets for 20% Pt/Ni$(HCO_3)_2$ gives rise to two pairs of peaks, where metallic Pt dominates in both doublets (Figure 2b).[12] The peak at 69 eV corresponds to Ni 3p of Ni$(HCO_3)_2$.[13] Notably, the binding energy (BE) of Pt $4f_{7/2}$ and Pt $4f_{5/2}$ upshifts by 0.25 and 0.22 eV, respectively. Similar behaviour is also found in 9% Pt/Ni$(HCO_3)_2$ (Figure S7d). The positive BE shift not only proves the presence of electronic interaction in the heterostructure,[14] but also suggests the downshift of *d*-band center of Pt in the heterostructure as compared with Pt NPs.[15] It is well established that the *d*-band center position can be used as a descriptor for the strength of the surface atom-adsorbate interaction.[16] And the downshift of the *d*-band center is convinced to induce the decrease of hydrogen binding energy,[16a, 17] which leads to a moderate Pt–H_{ad} (adsorbed hydrogen) binding energy, thus facilitating the recombination of H_{ad} to generate H_2.[17] Furthermore, evident BE shift is detected from the high-resolution C 1s spectra (Figure 2c and Figure S7e), and the assignment of the fitted C 1s core-level positions are listed in Table S1 (Supporting Information). The pristine Ni$(HCO_3)_2$ exhibits an intense peak at 290 eV (HCO_3^-), and two weak peaks at 286.2 (C–O) and 284.8 eV (C–C/C–H), respectively.[18] While the peak at 290 eV splits into two peaks at 290.1 and 288.6 eV (O–C=O),[19] respectively, for Pt/Ni$(HCO_3)_2$ heterostructures. Note that the BE of O–C=O downshifts after Pt deposition, which can be attributed to the strong chemical bonding and electronic interaction between Pt and Ni$(HCO_3)_2$. And the electron transfer from Pt NPs to Ni$(HCO_3)_2$ makes Ni$(HCO_3)_2$ with enriched electron density, which has an positive influence on the H_2O binding energy, resulting in accelerated water dissociation rate.[14] Besides, Pt–O–C=O bond is supposed to be formed considering the dramatic BE downshift (1 eV).[19a, 20] The high-resolution O 1s XPS spectra are also deconvolved (Figure 2d and Figure S7f). The peak at 532.8 eV can be assigned to Pt–O–C=O,[20-21] which upshifts by 0.4 eV for 20% Pt/Ni$(HCO_3)_2$ and 0.32 eV for 9% Pt/Ni$(HCO_3)_2$ as compared with Ni$(HCO_3)_2$. The strong BE shift can be ascribed to the Pt–O–C=O bond formation and electronic interaction, which is in agreement with the O–C=O BE downshift in C 1s spectra. The peak at 532 eV is attributed to hydroxyl group or the absorbed H_2O on the surface,[20-21] and the peak at 531.2 eV can be ascribed to C=O bond.[21a, 22] It should be mentioned that the core-level positions of Ni 2p keep unchanged after Pt grown on Ni$(HCO_3)_2$ (Figure S7g and h), suggesting that there is no change in the electronic structure of Ni (II). Based on the aforementioned discussion, we suppose that Pt NPs might be attached to Ni$(HCO_3)_2$ via Pt–O–C=O covalent bond.

To further investigate the coordination structure of Pt species in the heterostructure, the Pt L_3-edge X-ray absorption near edge structure (XANES) and extended X-ray absorption fine structure (EXAFS) spectra were investigated. As shown in Figure 2e, the white line (WL) intensity reflects the oxidation state of Pt species. It is clear that the WL intensities increase in the order of Pt foil< Pt NPs< Pt/Ni$(HCO_3)_2$, indicating that Pt in the heterostructure carries more positive charges and electrons transfer from Pt to Ni$(HCO_3)_2$,[23] which is in accordance with XPS analysis (Figure 2b-d). Figure 2f exhibits the Fourier transforms of the Pt L_3-edge EXAFS oscillations. The main peak at 2-3 Å arises from Pt–Pt bonding, and the relative intensity of Pt/Ni$(HCO_3)_2$ is extremely weaker than that of Pt NPs, revealing weaker Pt–Pt coordination in the heterostructure.[23b, 24] Notably, Pt/Ni$(HCO_3)_2$ shows a stronger peak at 1.6 Å, which can be assigned to Pt–O coordination.[23b, 24] Moreover, the wavelet transform (WT) analysis, which provides a radial distance resolution and the resolution in the k space, was performed. As shown in Figure S8, the WT intensity maximums are detected at similar k position (at ~9 $Å^{-1}$) for both Pt and Pt/Ni$(HCO_3)_2$, which can be identified as Pt–Pt coordination.[23b] In addition, a pre-WT intensity at 5.5 $Å^{-1}$ is detected only for Pt/Ni$(HCO_3)_2$, which is due to the Pt–O bonding.[23b, 25] Further quantitative EXAFS curve fitting analysis reveals that the coordination number of Pt–Pt in Pt NPs is 7.5 at the distance of 2.75 Å, while it decreases to 6.6 at 2.73 Å in

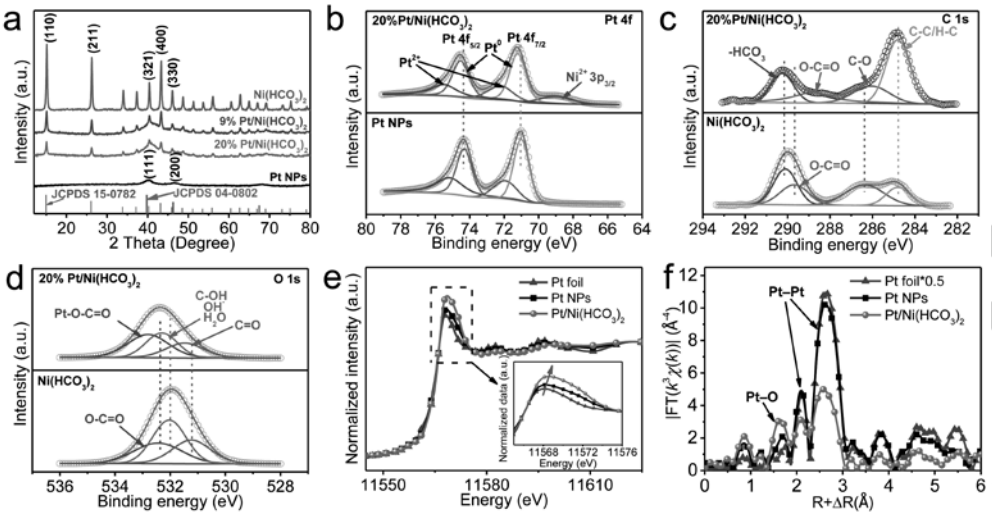

Figure 2. a) XRD patterns of the as-prepared Pt/Ni(HCO_3)$_2$ heterostructures, bare Pt and Ni(HCO_3)$_2$. b-d) High-resolution XPS spectra of Pt 4f for 20% Pt/Ni(HCO_3)$_2$ and bare Pt (b), C 1s (c) and O 1s (d) for 20% Pt/Ni(HCO_3)$_2$ heterostructure and Ni(HCO_3)$_2$. e) Pt L_3-edge XANES spectra (inset: enlarged spectra at Pt L_3 edge), and f) Pt L_3-edge k^3-weight FT-EXAFS spectra of Pt foil, Pt NPs and Pt/Ni(HCO_3)$_2$ heterostructure.

Pt/Ni(HCO_3)$_2$. And Pt–O coordination number in Pt/Ni(HCO_3)$_2$ is 1.2 at 2.09 Å (Table S2). The abundant Pt–O bonds evidenced by XANES and EXAFS further confirm a strong interaction between Pt and Ni(HCO_3)$_2$, which would in turn modulate the catalytic activity of the Pt/Ni(HCO_3)$_2$ heterostructures.

The geometric linear sweep voltammetry (LSV) curves (**Figure 3**a) reveal that Ni(HCO_3)$_2$ is absolutely inert for HER, while 20% Pt/Ni(HCO_3)$_2$ and bare Pt NPs exhibit superior HER activity with low Tafel slops and low overpotentials (η) (Figure 3b and Figure S9a) over 10% Pt/C, 9% Pt/Ni(HCO_3)$_2$ and 20% Pt+Ni(HCO_3)$_2$ (20 wt% Pt NPs physically mixed with Ni(HCO_3)$_2$). It has to be noted that, the real mass loading of Pt is 40, 8, 3.6, 8 and 4 μg for bare Pt NPs, 20% Pt/Ni(HCO_3)$_2$, 9% Pt/Ni(HCO_3)$_2$, 20% Pt+Ni(HCO_3)$_2$ and 10% Pt/C, respectively. Therefore, the geometric LSV curves cannot scientifically reflect their authentic HER activity. As shown in Figure S10a-d, the catalytic activity of Pt NPs varies dramatically with different bare Pt mass loadings. Accordingly, 20% Pt/Ni(HCO_3)$_2$ demonstrates superior catalytic activity to Pt NPs with the same Pt loading. The result uncovers that Ni(HCO_3)$_2$ plays a critical role in promoting the alkaline HER kinetics of Pt. To solve the aforementioned discrepancy, the specific activity with current densities (j) normalized by the relative electrochemical active surface area (ECSA) is discussed (Figure 3c and d). In this work, the double-layer capacitance (C_{dl}) of the samples in the non-Faraday region was measured to represent ECSA (**Figure 4**a and Figure S11). Bare Pt NPs exhibit the highest C_{dl} because of its highest Pt mass loading. It is clear that 20% Pt/Ni(HCO_3)$_2$ exhibits enhanced relative ECSA normalized HER activity and faster reaction kinetics than that of bare Pt NPs and 10% Pt/C. Remarkably, the η is as low as 27 mV for 20% Pt/Ni(HCO_3)$_2$ to achieve the j of 10 mA cm^{-2}, which is 17 mV lower than that of bare Pt electrode, and the performance difference is much evident when j reaches 50 mA cm^{-2} (Figure S9b). Notably, 9% Pt/Ni(HCO_3)$_2$ and 20% Pt+Ni(HCO_3)$_2$ also show higher catalytic activity over Pt NPs, which should be closely associated with Ni(HCO_3)$_2$. Besides, the superior activity of 20% Pt/Ni(HCO_3)$_2$ over 20% Pt+Ni(HCO_3)$_2$ reveals that the interaction between Pt and Ni(HCO_3)$_2$ is of great importance to the accelerated alkaline HER kinetics. In addition, the alkaline HER performance of Pt/Ni(HCO_3)$_2$ heterostructures with different Pt loadings and bare Pt NPs are presented in Figure S12. It is obvious that 20% is an optimized weight ratio to achieve the balance of the exposed Ni(HCO_3)$_2$ surface and uniformly dispersed Pt active sites for accelerated alkaline HER kinetics. The LSV curves normalized by Pt mass are also investigated (Figure S13). A high mass specific j of 1.77 mA μg_{Pt}^{-1} can be achieved for 20% Pt/Ni(HCO_3)$_2$ at the η of 100 mV, which is substantially higher than those of other samples. 20% Pt/Ni(HCO_3)$_2$ also outperforms some reported Pt-based catalysts towards alkaline HER (Table S3).

The intrinsic activity is depicted by the relative ECSA normalized exchange current densities ($j_{0,normalized}$) (Figure S14 and Table S4). 20% Pt/Ni(HCO_3)$_2$ and 9% Pt/Ni(HCO_3)$_2$ exhibit high $j_{0,normalized}$ of 5.6 and 5 mA cm^{-2}, respectively, which are much higher than that of bare Pt NPs (2.8 mA cm^{-2}). The significant increment of j_0

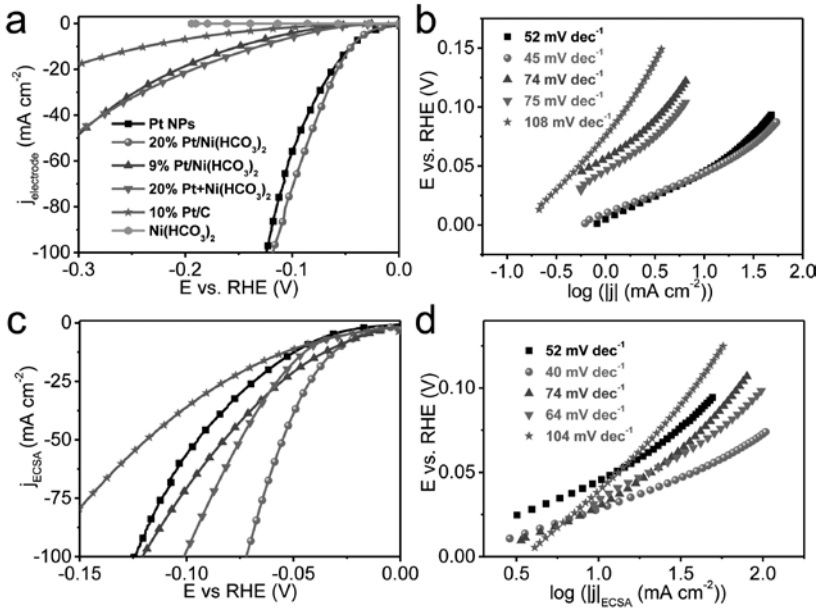

Figure 3. a) Geometric LSV curves and b) the corresponding Tafel plots of bare Pt, 20% Pt/Ni(HCO_3)$_2$, 9% Pt/Ni(HCO_3)$_2$, 20% Pt+Ni(HCO_3)$_2$, commercial 10% Pt/C and Ni(HCO_3)$_2$ measured in 1 M KOH aqueous solution. c) Relative ECSA normalized LSV curves and d) the corresponding Tafel plots of bare Pt, 20% Pt/Ni(HCO_3)$_2$, 9% Pt/Ni(HCO_3)$_2$, 20% Pt+Ni(HCO_3)$_2$ and commercial 10% Pt/C.

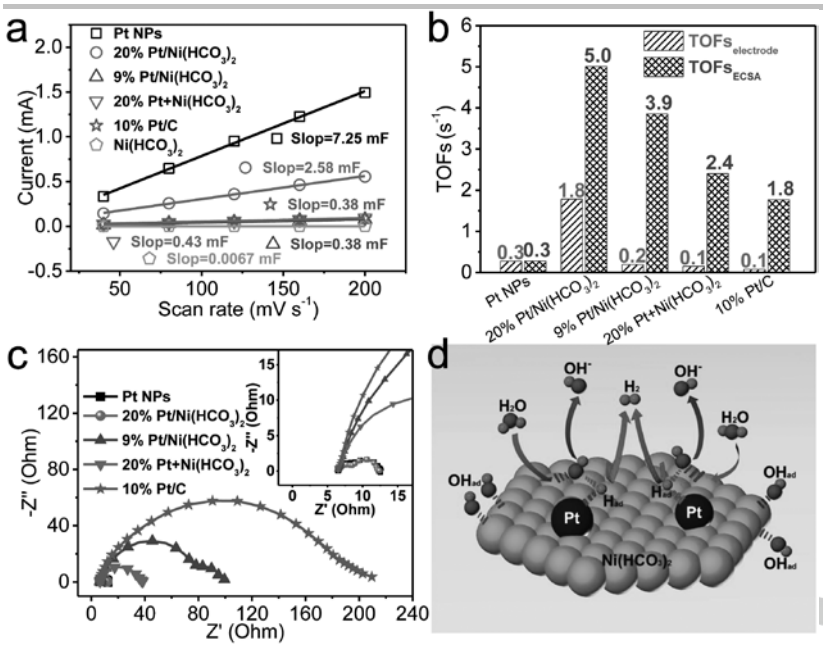

Figure 4. a) The current difference (j_a-j_c)/2 at 50 mV plotted against scan rate, the C_{dl} values are derived by linear fitting the plots, b) TOF values derived from the geometric and relative ECSA normalized TOF values at the η of 100 mV and c) EIS plots measured at the η of 100 mV for bare Pt, 20% Pt/Ni(HCO_3)$_2$, 9% Pt/Ni(HCO_3)$_2$, 20% Pt+Ni(HCO_3)$_2$ and commercial 10% Pt/C (Inset: enlarged EIS plots). d) Schematic illustration of a possible electrocatalytic mechanism to explain the enhanced HER activity of Pt/Ni(HCO_3)$_2$ heterostructures in alkaline medium.

confirms the accelerated electron transfer rate. Turnover frequency (TOF) is also an important parameter to evaluate the intrinsic activity. 20% Pt/Ni(HCO_3)$_2$ delivers the highest TOF value (1.8 s^{-1}) among the samples (Figure 4b and Figure S15a). And the superiority of Pt/Ni(HCO_3)$_2$ becomes more distinguished when TOF is normalized by relative ECSA (Figure S15b). The electrochemical impedance spectroscopy (EIS) in Figure 4c shows that 20% Pt/Ni(HCO_3)$_2$ (6 Ω) and Pt NPs (5.6 Ω) deliver extremely lower reaction resistances as compared to other samples. High Pt mass loading is beneficial to enhance electron transfer. On the other hand, the presence of hydrophilic Ni(HCO_3)$_2$ and the strong interaction in the heterostructures may facilitate the diffusion of the reactants and intermediates during the electrochemical reactions. Moreover, the synergistic effect ensures 20% Pt/Ni(HCO_3)$_2$ to show fast charge transfer and mass diffusion, thereby inducing accelerated hydrogen evolution kinetics. Finally, the performance stability (Figure S16a) shows that 20% Pt/Ni(HCO_3)$_2$ preserves 83% of its initial current, while bare Pt NPs and 20% Pt+Ni(HCO_3)$_2$ only maintain 62% after a 3-h test. The Ni(HCO_3)$_2$ could efficiently prevent the aggregation of Pt NPs with the help of strong coupling with Pt, thus ensuring the heterostructure with higher durability. The good structural stability is also evidenced by the TEM images of 20% Pt/Ni(HCO_3)$_2$ after 50 cyclic voltammetry test (Figure S16b and c). Figure 4d illustrates a possible mechanism for the enhanced alkaline HER activity of Pt/Ni(HCO_3)$_2$. Ni(HCO_3)$_2$ acts as an efficient role for H_2O adsorption/dissociation and consequently promotes the Volmer step ($H_2O+e^- \rightarrow H_{ad}+OH^-$), and Pt serves as the active center for H_{ad} adsorption/recombination via the Heyrovsky step ($H_2O+e^-+H_{ad} \rightarrow H_2+OH^-$) and/or Tafel step ($H_{ad}+H_{ad} \rightarrow H_2$). Ni($HCO_3$)$_2$ also helps to accelerate the following Heyrovsky step, where H_2O dissociation is also involved. Notably, the water dissociation by-product OH^- prefers to adsorbing to the Ni(HCO_3)$_2$ surface, which would protect Pt surface from being occupied by OH^-, maintaining active sites for H adsorption and thus facilitating hydrogen evolution.[26] On the other hand, the unique heterostructure with well-defined interface ensures the maximal exposure of Pt active sites, and the strong electronic interaction between Pt and Ni(HCO_3)$_2$ optimizes the H_{ad} affinity of Pt species, both of which would greatly accelerate the Heyrovsky and/or Tafel steps, thereby promoting H_{ad} recombination to generate H_2.

In summary, Pt/Ni(HCO_3)$_2$ hetero-nanostructures were designed towards accelerated alkaline HER kinetics. Electrochemically inert Ni(HCO_3)$_2$ was, for the first time, demonstrated to be an efficient catalyst promoter with decent water adsorption/dissociation capability for alkaline HER. Ni(HCO_3)$_2$ also plays an active role in preventing the growth and agglomeration of Pt NPs, thus ensuring the maximal exposure of Pt active sites. Also, the strong coupling between Ni(HCO_3)$_2$ and Pt induces intensive electronic interaction, and the H_{ad} affinity of Pt is optimized accordingly. Benefiting from the aforementioned unique functionalities, Pt/Ni(HCO_3)$_2$ exhibits remarkably enhanced alkaline HER activity and stability. The results demonstrate that engineering heterostructures is an effective strategy towards the development of efficient catalysts.

Acknowledgements

This work was financially supported by Australian Research Council (ARC) DECRA Grant (DE160100596), AIIM FOR GOLD Grant (2017, 2018) and National Natural Science Foundation of China (Grant no. 11875258, 11505187 and 41701359). The authors also acknowledge use of facilities within the UOW Electron Microscopy Centre and the staff of beamline BL14W1 at Shanghai Synchrotron Radiation Facility for their support in XAFS measurements.

Keywords: heterostructure • platinum • nickel bicarbonate • hydrogen evolution reaction • synergistic effect

[1] a) E. Pomerantseva, Y. Gogotsi, *Nat. Energy* **2017**, *2*, 17089-17094; b) K. S. Novoselov, A. Mishchenko, A. Carvalho, A. H. Castro Neto, *Science* **2016**, *353*, 461-473.

[2] H. Jin, C. Guo, X. Liu, J. Liu, A. Vasileff, Y. Jiao, Y. Zheng, S. Z. Qiao, *Chem. Rev.* **2018**, *118*, 6337-6408.

[3] J. Mei, Y. Zhang, T. Liao, Z. Sun, S. X. Dou, *Natl. Sci. Rev.* **2018**, *5*, 389-416.

[4] a) H. Fan, H. Yu, Y. Zhang, Y. Zheng, Y. Luo, Z. Dai, B. Li, Y. Zong, Q. Yan, *Angew. Chem. Int. Ed.* **2017**, *56*, 12566-12570; b) Y. Li, Z. Wang, T. Xia, H. Ju, K. Zhang, R. Long, Q. Xu, C. Wang, L. Song, J. Zhu, J. Jiang, Y. Xiong, *Adv. Mater.* **2016**, *28*, 6959-6965; c) J. X. Feng, H. Xu, Y. T. Dong, X. F. Lu, Y. X. Tong, G. R. Li, *Angew. Chem. Int. Ed.* **2017**, *56*, 2960-2964; d) J. X. Feng, S. Y. Tong, Y. X. Tong, G. R. Li, *J. Am. Chem. Soc.*

2018, *140*, 5118-5126; e) J. X. Feng, J. Q. Wu, Y. X. Tong, G. R. Li, *J. Am. Chem. Soc.* **2018**, *140*, 610-617.

[5] W. Sheng, Z. Zhuang, M. Gao, J. Zheng, J. G. Chen, Y. Yan, *Nat. Commun.* **2015**, *6*, 5848-5853.

[6] N. Mahmood, Y. Yao, J. W. Zhang, L. Pan, X. Zhang, J. J. Zou, *Adv. Sci.* **2018**, *5*, 1700464-1700486.

[7] a) M. A. Henderson, *Surf. Sci. Rep.* **2002**, *46*, 1-308; b) Z. Zhu, H. Yin, C. T. He, M. Al-Mamun, P. Liu, L. Jiang, Y. Zhao, Y. Wang, H. G. Yang, Z. Tang, D. Wang, X. M. Chen, H. Zhao, *Adv. Mater.* **2018**, *30*, 1801171-1801177.

[8] N. Danilovic, R. Subbaraman, D. Strmcnik, K. C. Chang, A. P. Paulikas, V. R. Stamenkovic, N. M. Markovic, *Angew. Chem. Int. Ed.* **2012**, *51*, 12495-12498.

[9] a) Z.-J. Chen, G.-X. Cao, L.-Y. Gan, H. Dai, N. Xu, M.-J. Zang, H.-B. Dai, H. Wu, P. Wang, *ACS Catal.* **2018**, *8*, 8866-8872; b) L. Wang, Y. Zhu, Z. Zeng, C. Lin, M. Giroux, L. Jiang, Y. Han, J. Greeley, C. Wang, J. Jin, *Nano Energy* **2017**, *31*, 456-461.

[10] N. T. Suen, S. F. Hung, Q. Quan, N. Zhang, Y. J. Xu, H. M. Chen, *Chem. Soc. Rev.* **2017**, *46*, 337-365.

[11] S. Chen, J. Duan, M. Jaroniec, S. Z. Qiao, *Adv. Mater.* **2014**, *26*, 2925-2930.

[12] D. Skomski, C. D. Tempas, K. A. Smith, S. L. Tait, *J. Am. Chem. Soc.* **2014**, *136*, 9862-9865.

[13] H. Yin, S. Zhao, K. Zhao, A. Muqsit, H. Tang, L. Chang, H. Zhao, Y. Gao, Z. Tang, *Nat. Commun.* **2015**, *6*, 6430-6437.

[14] S. Yin, W. Tu, Y. Sheng, Y. Du, M. Kraft, A. Borgna, R. Xu, *Adv. Mater.* **2017**, 1705106-1705114.

[15] a) B. Y. Xia, H. B. Wu, N. Li, Y. Yan, X. W. Lou, X. Wang, *Angew. Chem. Int. Ed.* **2015**, *54*, 3797-3801; b) M. Wakisaka, S. Mitsui, Y. Hirose, K. Kawashima, H. Uchida, M. Watanabe, *J. Phys. Chem. B* **2006**, *110*, 23489-23496.

[16] a) V. R. Stamenkovic, B. S. Mun, M. Arenz, K. J. Mayrhofer, C. A. Lucas, G. Wang, P. N. Ross, N. M. Markovic, *Nat. Mater.* **2007**, *6*, 241-247; b) J. Greeley, J. K. Norskov, M. Mavrikakis, *Annu. Rev. Phys. Chem.* **2002**, *53*, 319-348.

[17] W. F. Chen, K. Sasaki, C. Ma, A. I. Frenkel, N. Marinkovic, J. T. Muckerman, Y. Zhu, R. R. Adzic, *Angew. Chem. Int. Ed.* **2012**, *51*, 6131-6135.

[18] a) Y. Wei, G. Cheng, J. Xiong, F. Xu, R. Chen, *ACS Sustainable Chem. Eng.* **2017**, *5*, 5027-5038; b) S. Zhao, Z. Wang, Y. He, B. Jiang, Y. Harn, X. Liu, F. Yu, F. Feng, Q. Shen, Z. Lin, *ACS Energy Lett.* **2016**, *2*, 111-116.

[19] a) M. Xing, F. Shen, B. Qiu, J. Zhang, *Sci. Rep.* **2014**, *4*, 6341-6347; b) J. Senthilnathan, Y. F. Liu, K. S. Rao, M. Yoshimura, *Sci. Rep.* **2014**, *4*, 4395-4401.

[20] N. Wang, J. Liu, W. Gu, Y. Song, F. Wang, *RSC Adv.* **2016**, *6*, 77786-77795.

[21] a) M. Leng, X. Huang, W. Xiao, J. Ding, B. Liu, Y. Du, J. Xue, *Nano Energy* **2017**, *33*, 445-452; b) J. Liu, J. Liu, W. Song, F. Wang, Y. Song, *J. Mater. Chem. A* **2014**, *2*, 17477-17488.

[22] Z. Yang, J. Lv, H. Pang, W. Yan, K. Qian, T. Guo, Z. Guo, *Sci. Rep.* **2015**, *5*, 17473-17482.

[23] a) X. Cheng, Y. Li, L. Zheng, Y. Yan, Y. Zhang, G. Chen, S. Sun, J. Zhang, *Energy Environ. Sci.* **2017**, *10*, 2450-2458; b) H. Zhang, P. An, W. Zhou, B. Y. Guan, P. Zhang, J. Dong, X. W. D. Lou, *Sci. Adv.* **2018**, *4*, 1-9.

[24] K. Zhang, W. Yang, C. Ma, Y. Wang, C. Sun, Y. Chen, P. Duchesne, J. Zhou, J. Wang, Y. Hu, M. N. Banis, P. Zhang, F. Li, J. Li, L. Chen, *NPG Asia Mater.* **2015**, *7*, e153-e162.

[25] T. He, S. Chen, B. Ni, Y. Gong, Z. Wu, L. Song, L. Gu, W. Hu, X. Wang, *Angew. Chem. Int. Ed.* **2018**, *57*, 3493-3498.

[26] M. Gong, W. Zhou, M. C. Tsai, J. Zhou, M. Guan, M. C. Lin, B. Zhang, Y. Hu, D. Y. Wang, J. Yang, S. J. Pennycook, B. J. Hwang, H. Dai, *Nat. Commun.* **2014**, *5*, 4695-4700.

Entry for the Table of Contents (Please choose one layout)

Layout 1:

COMMUNICATION

New $Pt/Ni(HCO_3)_2$ heterostructures are designed and synthesized towards accelerated alkaline hydrogen evolution reaction (HER). The significantly enhanced HER activity can be ascribed to the accelerated water dissociation, the optimized hydrogen affinity and the abundant active sites of the heterostructures.

Mengmeng Lao, Kun Rui, Guoqiang Zhao, Peixin Cui, Xusheng Zheng, Shi Xue Dou and Wenping Sun**

Page No. – Page No.

Platinum/Nickel Bicarbonate Heterostructures towards Accelerated Alkaline Hydrogen Evolution Reaction